

Modeling Aeolian Sediment Supply at a Mega Nourishment

Bas Hoonhout^{a,b,*}, Sierd de Vries^b



^a*Deltares, Department of Hydraulic Engineering, Boussinesqweg 1, 2629HV Delft, The Netherlands.*

^b*Delft University of Technology, Faculty of Civil Engineering and Geosciences, Department of Hydraulic Engineering, Stevinweg 1, 2628CN Delft, The Netherlands.*

Abstract

Mega nourishments are a novel approach to coastal safety and resilience that intend to stimulate natural sediment transport processes on a decadal time scale with a minimum of intrusion into the natural coastal system. However, the supratidal morphodynamic behaviour of mega nourishments, relevant to both coastal safety and coastal landscape and habitat development, is not yet well understood due to complexities introduced by limitations in sediment availability.

In this paper we present a detailed 4-year hindcast of the Sand Motor mega nourishment in The Netherlands using the aeolian sediment transport and availability model AEOL that focuses specifically on the simulation of spatiotemporal variations in sediment availability, including the recurrence relation between sediment availability and aeolian sediment transport through self-grading and beach armoring.

We show that the model is quantitatively valuable and practically applicable as it is able to reproduce multi-annual aeolian sediment transport rates in the Sand Motor domain in the four years after its construction with a RMSE of $3 \cdot 10^4 \text{ m}^3$ and R^2 of 0.93. The combination of spatial and temporal variations in aeolian sediment availability, due to the combined influence of soil moisture, sediment sorting and beach armoring, and the feedback between aeolian sediment availability and transport is essential for an accurate estimate of the total sedimentation volume and the corresponding aeolian sediment source areas in the Sand Motor domain.

Keywords: aeolian sediment transport; aeolian sediment supply; beach armoring; mega nourishment; Sand Motor; numerical model; aeolis

*Corresponding author
Preprint submitted to Coastal Engineering
Email addresses: b.m.hoonhout@tudelft.nl (Bas Hoonhout),
bas.hoonhout@deltares.nl (Bas Hoonhout)

March 9, 2018

1. Introduction

Mega nourishments are a novel approach to coastal safety and resilience (Stive et al., 2013). Mega nourishments intend to stimulate natural sediment transport processes on a decadal time scale with a minimum of intrusion into the natural coastal system. By concentrating coastal interventions in both time and space, mega nourishments are believed to strengthen the natural coastal system and provide a cost-effective solution to coastal hazards that is flexible enough to cope with uncertainties associated with climate change, while stimulating natural coastal landscape and habitat development.

Nevertheless, mega nourishment tend to show particular morphodynamic behaviour, relevant to both coastal safety and coastal landscape and habitat development, that is not yet well understood (de Schipper et al., 2016; Huisman et al., 2016; Radermacher et al., 2017). Hoonhout and de Vries (2017) showed that the supratidal morphodynamic behavior of the Sand Motor mega nourishment in The Netherlands is highly compartmentalized, resulting in dune growth rates that are lower than along the adjacent coasts with more regular beaches. Despite fetches up to 1 kilometer, aeolian sediment transport rates remain modest due to limitations in sediment availability.

Aeolian sediment transport models systematically overestimate the actual aeolian sediment flux (Sherman et al., 1998; Sherman and Li, 2012), which can be accredited to limitations in sediment availability (e.g. Jackson and Cooper, 1999; Lynch et al., 2008; Davidson-Arnott and Bauer, 2009; Aagaard, 2014). However, implementation of availability limitations in aeolian sediment transport models is complicated as sediment availability is governed by a variety of environmental factors and inherently varies both in time and space. Hence, limitations in sediment availability also complicate the performance assessment of mega nourishments as measure to stimulate coastal safety and coastal landscape and habitat development. For unbiased assessment of these novel approaches to coastal safety and resilience with respect to alternative measures, quantification of the aeolian sediment flux in complex coastal configurations and availability-limited conditions is paramount.

Limitations in sediment availability are traditionally incorporated in formulations for equilibrium or saturated sediment transport through a shear velocity threshold (e.g. Howard, 1977; Dyer, 1986; Belly, 1964; Johnson, 1965; Hotta et al., 1984; Nickling and Ecclestone, 1981; Arens, 1996; King et al.,



68 2005). To incorporate the spatiotemporal variations in sediment availability,
69 various conceptual frameworks have been developed.

70 Bauer and Davidson-Arnott (2002) introduced the concept of critical fetch
71 to account for limitations in fetch and sediment availability and supply in
72 coastal sediment transport estimates. de Vries et al. (2014a) used an explicit
73 source term in a one-dimensional advection formulation to account for spa-
74 tial variations in sediment availability. Keijsers et al. (2016) introduced the
75 behavioral DUBEVEG model, as extension of the DECAL algorithm (Baas,
76 2002), that uses probabilities to account for spatiotemporal differences in
77 beach erosion, dune development and vegetation growth.

78 Although conceptually useful, these concepts have limited predictive ca-
79 pabilities as the critical fetch in Bauer and Davidson-Arnott (2002), the
80 explicit source term in de Vries et al. (2014a) and the probabilities in the
81 DUBEVEG model are typically unknown a-priori. Therefore, various process-
82 based frameworks have been developed to simulate the spatiotemporal vari-
83 ation in sediment availability. The simulated sediment availability can then
84 be fed to a aeolian sediment transport model to obtain aeolian sediment
85 transport fluxes for availability-limited coastal systems.

86 Van Dijk et al. (1999) and Van Boxel et al. (1999) introduced an ex-
87 tensive numerical model that simulates airflow over a given topography and
88 computes the spatiotemporal variation in aeolian sediment transport includ-
89 ing various limitations in sediment availability, like the effect of precipitation
90 and vegetation. Their model did not allow for simulation of the limitations
91 in sediment availability itself and appears to be computationally intensive
92 due to the flow solver. Kroy et al. (2002) introduced a more lightweight flow
93 solver based on the model of Weng et al. (1991). Durán and Moore (2013)
94 extended this model with a vegetation growth model and a water line to sim-
95 ulate the development of coastal dunes. However, their model is focused on
96 more traditional coastlines as limitations in sediment availability are included
97 only through vegetation.

98 Hoonhout and de Vries (2016) introduced the AEOLIS model that focuses
99 specifically on the simulation of spatiotemporal variations in sediment avail-
100 ability, including the recurrence relation between sediment availability and
101 aeolian sediment transport through self-grading and beach armoring. The
102 model can be used to obtain a lightweight, but versatile aeolian sediment
103 transport model that is suitable for availability-limited coastal environments.

104 Practical and versatile aeolian sediment transport models with predictive
105 skill are a prerequisite for design and optimization of mega nourishments on

106 their effectiveness to increase coastal safety and resilience, while stimulat-
107 ing natural coastal landscape and habitat development. To provide insight
108 in the predictive skill of models for the long-term development of the com-
109 plex coastal environments that mega nourishment typically are, long-term
110 validation taking into account the spatiotemporal differentiation of aeolian
111 sediment transport and availability is required.

112 In this paper we present a detailed 4-year hindcast of the Sand Motor
113 mega nourishment in The Netherlands using the aeolian sediment transport
114 and availability model of Hoonhout and de Vries (2016). We show that spa-
115 tiotemporal variations in sediment availability cause stabilization of the mega
116 nourishment and increase its lifetime significantly. We also show that both
117 spatial and temporal variability in sediment availability are key to explain
118 the long-term and seasonal morphodynamic behaviour of the nourishment.

119 2. Field Site

120 The Sand Motor (or Sand Engine) is an artificial 21 Mm³ sandy peninsula
121 protruding into the North Sea off the Delfland coast in The Netherlands
122 (Figure 1, Stive et al., 2013). The Sand Motor was constructed in 2011 and
123 its bulged shoreline initially extended about 1 km seaward and stretched
124 over approximately 2 km along the original coastline. The original coast was
125 characterized by an alongshore uniform profile with a vegetated dune with
126 an average height of 13 m and a linear beach with a 1:40 slope. The dune
127 foot is located at a height of approximately 5 m+MSL.

128 Due to natural sediment dynamics the Sand Motor distributes about 1
129 Mm³ of sand per year to the adjacent coasts (Figure 1). The majority of this
130 sand volume is transported by tides and waves. However, the Sand Motor
131 is constructed up to 5 m+MSL and locally up to 7 m+MSL, which is in
132 either case well above the maximum surge level of 3 m+MSL (Figure 2c).
133 Therefore, the majority of the Sand Motor area is uniquely shaped by wind.

134 The Sand Motor comprises both a dune lake and a lagoon that act as
135 large traps for aeolian sediment (Figure 1). The lagoon is affected by tidal
136 forcing, although the tidal amplitude quickly diminished over time as the
137 entry channel elongated. The tidal range of about 2 m that is present at the
138 Sand Motor periphery (Figure 2c), is nowadays damped to less than 20 cm
139 inside the lagoon (de Vries et al., 2015). Consequently, the tidal currents at
140 the closed end of the lagoon, where most aeolian sediment is trapped, are
141 negligible.

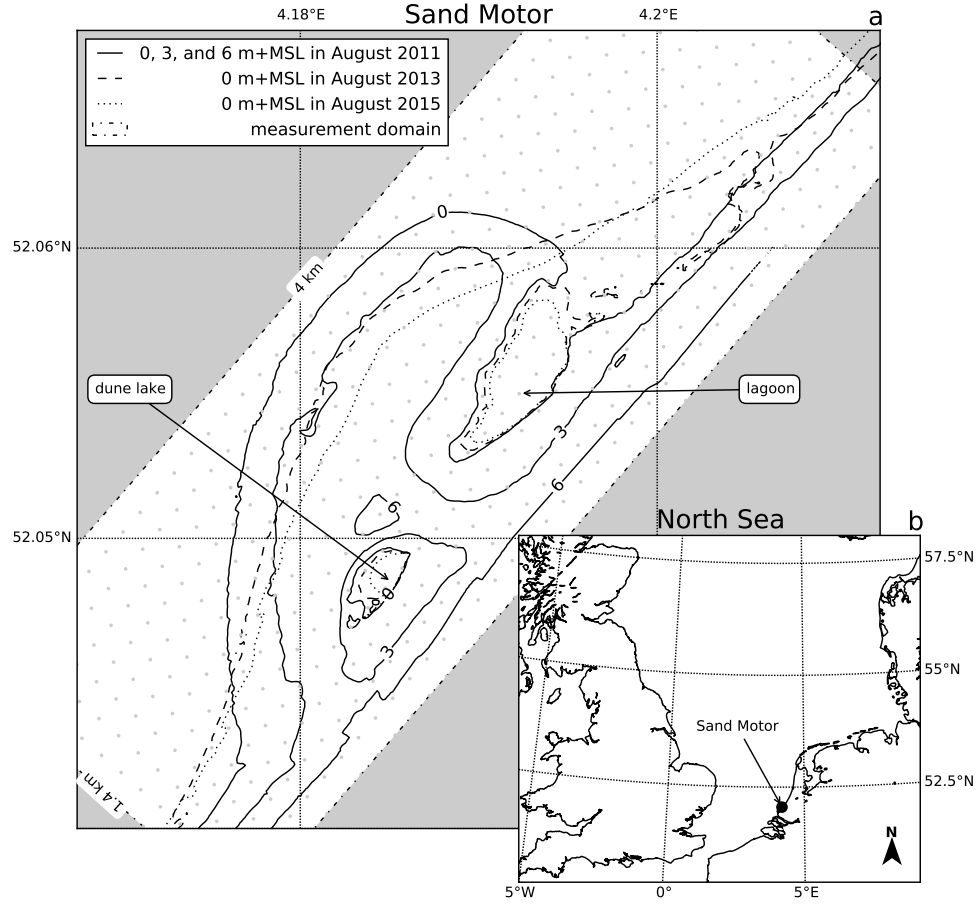


Figure 1: Location, orientation, appearance and evolution of the Sand Motor between construction in 2011 and 2015. The box indicates the measurement domain used in the remainder of this paper. A 100 x 100 m grid aligned with the measurement domain is plotted in gray as reference.

142 The dominant wind direction at the Sand Motor is south to southwest
 143 (Figure 2a). However, during storm conditions the wind direction tends to be
 144 southwest to northwest. During extreme storm conditions the wind direction
 145 tends to be northwest. Northwesterly storms are typically accompanied by
 146 significant surges as the fetch is virtually unbounded to the northwest, while
 147 surges from the southwest are limited due to the presence of the narrowing
 148 of the North Sea at the Strait of Dover (Figure 1, inset).

149 3. Model description

150 A two-dimensional (2DH) advection model for spatiotemporal varying
 151 aeolian sediment transport and availability is used (Hoonhout and de Vries,
 152 2016). The model simulates sediment availability through the processes of
 153 sediment sorting, beach armoring and flooding and drying. For this purpose
 154 the bed is discretized in horizontal grid cells and in vertical bed layers (2DV).
 155 Moreover, the grain size distribution is discretized into fractions. This allows
 156 the grain size distribution to vary both horizontally and vertically.

157 The model describes the instantaneous sediment mass per unit area in
 158 transport c [kg/m²] by an advection equation, which reads in one-dimensional
 159 notation:

$$\frac{\partial c_k}{\partial t} + u_z \frac{\partial c_k}{\partial x} = E_k - D_k \quad (1)$$

160 where t [s] denotes time, x [m] denotes the cross-shore distance from a zero-
 161 transport boundary, and k [-] denotes the sediment fraction index. u_z [m/s] is
 162 the wind velocity at height z [m]. E_k and D_k [kg/m²/s] represent the erosion
 163 and deposition terms and hence combined represent the net entrainment of
 164 sediment.

165 The net entrainment is determined based on a balance between the equi-
 166 librium or saturated sediment concentration $c_{\text{sat},k}$ [kg/m²] and the instanta-
 167 neous sediment transport concentration c_k and is maximized by the available
 168 sediment in the bed $m_{a,k}$ [kg/m²] according to:

$$E_k - D_k = \min \left(\frac{\partial m_{a,k}}{\partial t} ; \frac{\hat{w}_k \cdot c_{\text{sat},k} - c_k}{T} \right) \quad (2)$$

169 where T [s] represents an adaptation time scale that is assumed to be equal
 170 for both erosion and deposition. \hat{w}_k is a weighting factor that sums to unity
 171 over the grain size fractions. The saturated sediment concentration $c_{\text{sat},k}$ is

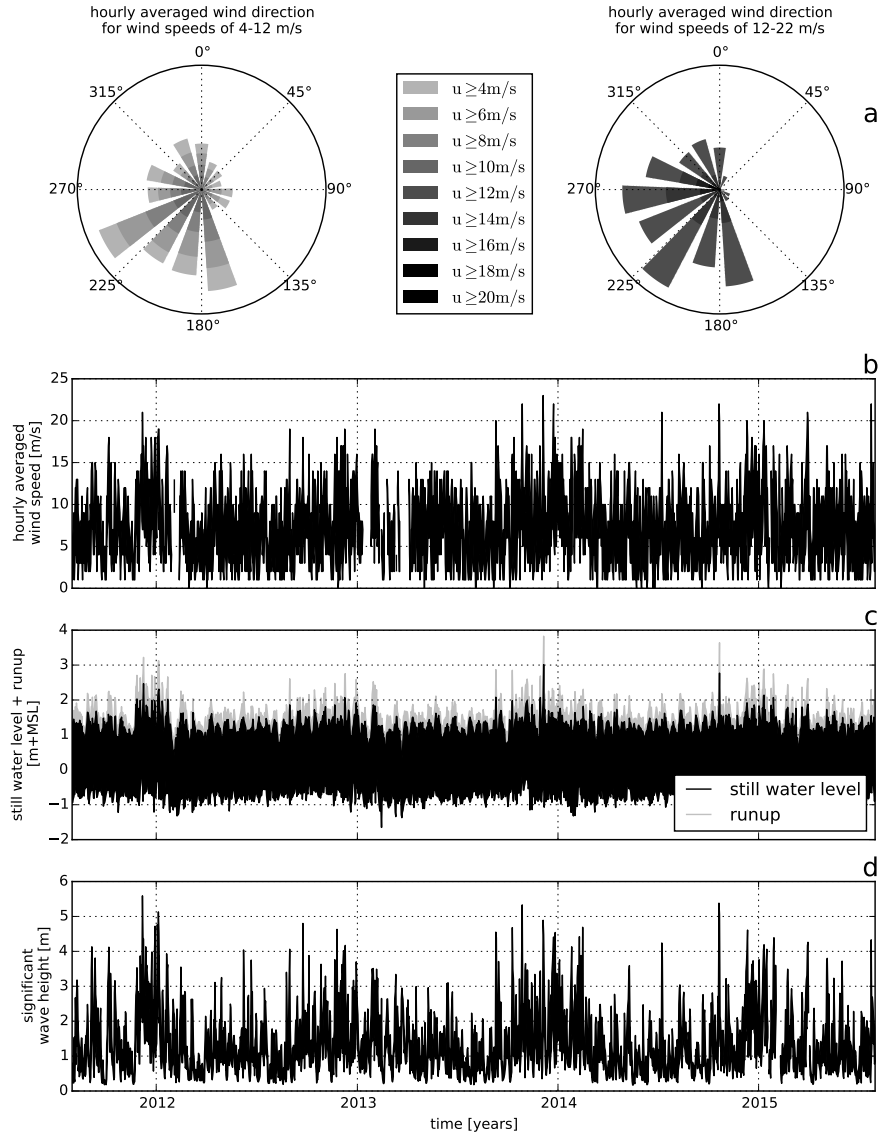


Figure 2: Wind and hydrodynamic time series from 2011 to 2015. Hourly averaged wind speeds and directions are obtained from the KNMI meteorological station in Hoek van Holland (upper panels). Offshore still water levels, wave heights and wave periods are obtained from the Europlatform (lower panels). Runup levels are estimated following Stockdon et al. (2006).

172 computed using an empirical sediment transport formulation (e.g. Bagnold,
173 1937).

174 The empirical sediment transport fomulation is provided with a term
175 for the shear velocity threshold $u_{*th,k}$ [m/s] that defines the minimum wind
176 shear required to initiate and sustain saltation transport. The shear velocity
177 threshold is determined based on bed surface properties, like soil moisture
178 content and the presence of roughness elements.

179 Saturation of the soil is assumed to be instantaneous with rising tide.
180 The drying of the beach surface through infiltration is assumed to follow an
181 exponential decay. In order to capture this behavior the volumetric water
182 content is implemented according to:

$$p_V = \begin{cases} p & \text{if } \eta > z_b \\ p \cdot \int e^{\frac{\log(0.5)}{T_{dry}} \cdot dt} & \text{if } \eta \leq z_b \end{cases} \quad (3)$$

183 where p [-] is the porosity, η [m+MSL] is the instantaneous water level, z_b
184 [m+MSL] is the local bed elevation, p_V [-] is the volumetric water content.
185 T_{dry} [s] is the beach drying time scale, defined as the time in which the beach
186 moisture content halves.

187 The sheltering effect of roughness elements protruding from the bed and
188 affecting the local wind shear and shielding local sediment is implemented
189 following Raupach et al. (1993):

$$f_{u_{*th,R}} = \sqrt{(1 - m\sigma\lambda)(1 + m\beta\lambda)} \quad (4)$$

190 where $f_{u_{*th,R}}$ [-] is a factor with which the local instantaneous shear velocity
191 threshold per sediment fraction is multiplied. λ [-] is the roughness density.
192 m , β and σ [-] are empirical factors defined in Raupach et al. (1993) rep-
193 resenting the difference between mean and maximum shear stress, the ratio
194 between the drag coefficient of the roughness elements alone and the drag
195 coefficient of the unarmored sandy bed, and the ratio between the basal and
196 frontal area of the roughness elements respectively.

197 4. Model approach

198 The two-dimensional (2DH) model of the Sand Motor is constructed and
199 calibrated based on four years of field measurements on wind, tides, waves
200 and topography. The calibrated model is used to investigate the influence of

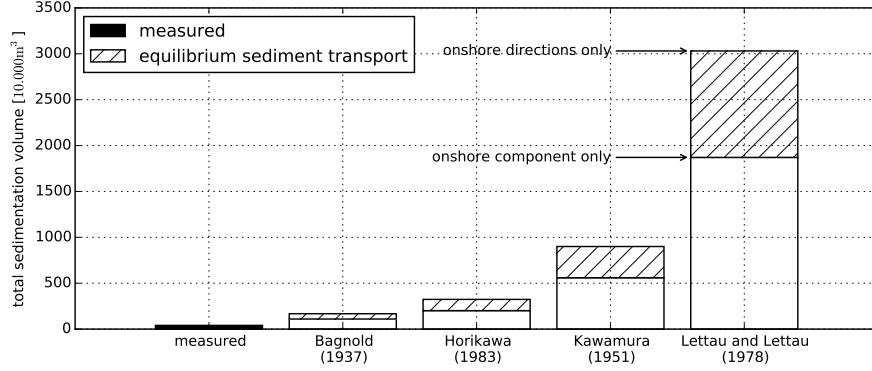


Figure 3: Comparison of the cumulative wind transport capacity according to a selection of equilibrium sediment transport formulations and measured total sedimentation in the Sand Motor domain. The equilibrium sediment transport is based on an hourly averaged wind speed and direction time series from September 1, 2011 until September 1, 2015. Offshore wind directions are discarded. For the upper boundary of each estimate all wind directions are weighted equally. For the lower boundary of each estimate the wind directions are weighted according to the magnitude of the onshore component.

201 spatiotemporal variations in aeolian sediment availability on sediment accu-
 202 mulation in the Sand Motor domain.

203 To test that the Sand Motor mega nourishment is indeed an availability-
 204 limited coastal system, the measured long-term sediment accumulation vol-
 205 umes (Hoonhout and de Vries, 2017) are first compared to a reference model
 206 that assumes no limitations in sediment availability exist.

207 4.1. Reference model

208 A selection of equilibrium sediment transport formulations is used as
 209 reference model. An equilibrium sediment transport formulation describes
 210 the wind transport capacity in given conditions. In conjunction with a
 211 shear velocity threshold based on only a constant uniform median grain size,
 212 an estimate of the potential aeolian sediment accumulation in absence of
 213 availability-limitations can be obtained. The potential aeolian sediment ac-
 214 cumulation or cumulative wind transport capacity Q [m^3] in the Sand Motor
 215 domain is estimated based on hourly averaged time series of the wind speed
 216 u_z [m/s] and direction θ_u [$^\circ$] obtained from the KNMI meteorological station
 217 in Hoek van Holland following:

$$Q = \sum q \cdot \frac{\Delta t \cdot \Delta y}{(1 - p) \cdot \rho_p} \cdot f_{\theta_u} \quad (5)$$

218 where the temporal resolution $\Delta t = 1$ h, the alongshore span of the domain
 219 $\Delta y = 4$ km, the porosity $p = 0.4$, the particle density $\rho_p = 2650$ kg/m³,
 220 the sediment transport rate q is given by the equilibrium sediment transport
 221 formulation (Table 1) and f_{θ_u} is a factor to account for the wind direction.
 222 The wind direction can be accounted for by only including the onshore wind
 223 component with respect to the original coastline orientation. However, given
 224 the typical Sand Motor geometry (Figure 1), sediment is likely to be trapped
 225 in the dune lake and lagoon even with alongshore wind. Therefore it can
 226 be assumed that the onshore wind component will provide a lower limit of
 227 the cumulative wind transport capacity. Similarly, an upper limit can be
 228 obtained by assuming that all onshore wind directions contribute equally to
 229 the cumulative wind transport capacity. For the upper limit the factor f_{θ_u}
 230 is defined as:

$$f_{\theta_u} = \begin{cases} 1 & \text{if } \cos(312^\circ - \theta_u) \geq 0 \\ 0 & \text{if } \cos(312^\circ - \theta_u) < 0 \end{cases} \quad (6)$$

231 while for the lower limit the factor f_{θ_u} is defined as:

$$f_{\theta_u} = \max(0 ; \cos(312^\circ - \theta_u)) \quad (7)$$

232 where 312° accounts for orientation of the original coastline. Figure 3 presents
 233 an overview of the cumulative wind transport capacity in the Sand Motor
 234 domain over the period between September 1, 2011 and September 1, 2015
 235 according to a selection of equilibrium sediment transport formulations and
 236 in comparison with the measured accumulation volumes. The estimates of
 237 the wind transport capacity show a large variation between formulations that
 238 are mainly due to the incorporation of the shear velocity threshold. How-
 239 ever, all formulations overestimate the measured sediment accumulation in
 240 the Sand Motor domain with at least a factor 3 – 4. The large variation and
 241 consistent overestimation is in accordance with the review of aeolian sedi-
 242 ment transport models presented by Sherman and Li (2012). The consistent
 243 overestimation of the measured sedimentation volumes in the Sand Motor
 244 domain suggest that the Sand Motor is indeed an availability-limited coastal
 245 system.

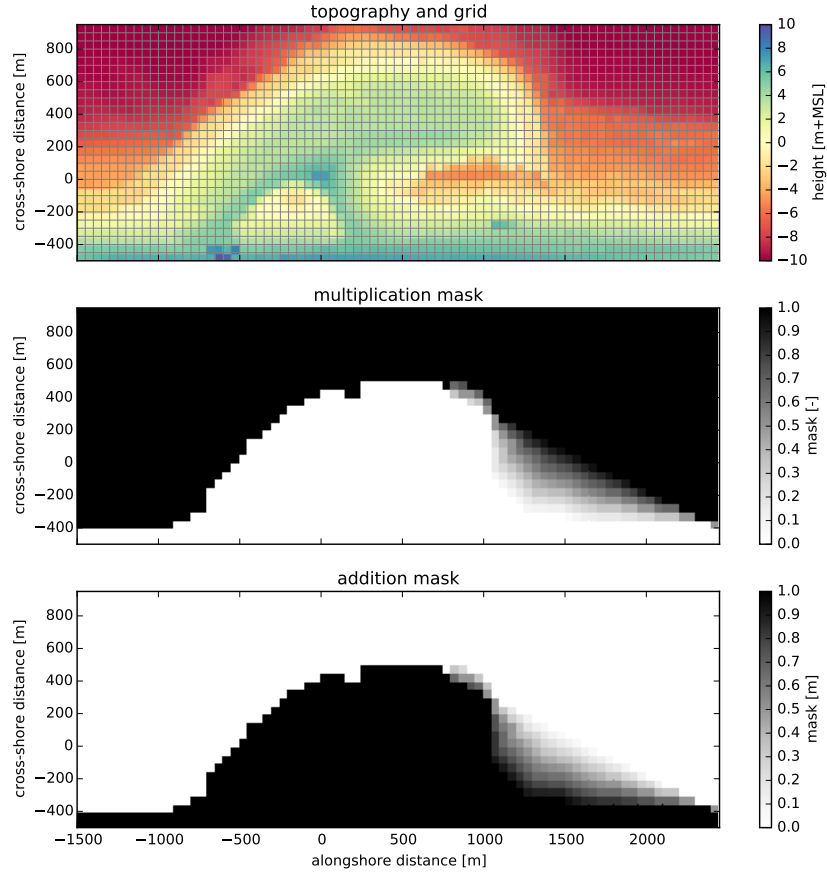


Figure 4: Model grid and topography based on the topographic survey of August 3, 2011 (upper panel) and hydrodynamic mask used to limit tidal and wave motions in the dune lake and lagoon (middle and lower panels). Water levels and wave heights are uniformly imposed to the model and multiplied by the multiplication mask and subsequently increased with the addition mask.

246 4.2. Schematization

247 A two-dimensional (2DH) aeolian sediment availability and transport
248 model for the Sand Motor mega nourishment is constructed for the four years
249 between September 1, 2011 and September 1, 2015, which is shortly after the
250 nourishment was placed. The model's topography and grid are based on the
251 measured topographies of August 3, 2011 and later. The topographies are
252 rotated 48° and interpolated to a 50 x 50 m grid spanning 1.5 km cross-shore
253 and 4 km alongshore with respect to the original coastline, not including the
254 dunes (Figure 4, upper panel).

255 Four years of hourly wind speed and direction data measured at 10 m
256 above the bed is obtained from the KNMI meteorological station at Hoek
257 van Holland (Figure 2a,b). Hourly offshore water levels and wave heights are
258 obtained from the Europlatform for the same period (Figure 2c,d).

259 An average lognormal grain size distribution with a median diameter
260 $d_{50} = 335 \mu\text{m}$ is used as measured at the Sand Motor field site. The sand
261 fractions cover a range from 0.1 to 2 mm. The amount of shells and other
262 roughness elements in the originally nourished sand is estimated to be 5%.
263 The estimate is based on three sediment samples obtained from the field
264 site 0.5 m below the bed surface. Additional fractions ranging from 2 to
265 32 mm are added according to a lognormal distribution to account for the
266 presence of roughness elements in the bed. The grain size distribution is used
267 to populate the initial bed that consists of 10 bed composition layers with a
268 thickness of 1 cm each.

269 The hindcast aims at the large scale and long term sedimentation volumes
270 as presented by Hoonhout and de Vries (2017). Therefore an efficient, but
271 diffusive, implicit Euler Backward scheme with a timestep of 1 h is used that
272 does not resolve high frequency variations in wind or sediment transport.
273 Consequently, the model produces smooth solutions that describe hourly
274 steady states based on the instantaneous average wind speed and sediment
275 availability.

276 Bagnold (1937) is selected as equilibrium sediment transport formulation
277 as it is derived separately for different grain sizes and therefore suitable for
278 multi-fraction aeolian sediment transport. Alternative formulations (Table 1)
279 are derived for wider grain size distributions that do not necessarily result in
280 a monotonic relation between the grain size and the sediment transport rate
281 (e.g. Kawamura, 1951; Horikawa et al., 1983). Such non-monotonic relation
282 is unrealistic in a multi-fraction context as it would result in a preference

Table 1: Equilibrium sediment transport formulations, coefficient values* and the ratio between measurements and model results.

Reference	Equation	C	Ratio
Bagnold (1937)	$q = C \frac{\rho_a}{g} \sqrt{\frac{d_n}{D_n}} (u_* - u_{*th})^3$	1.8	3 – 4
Horikawa et al. (1983)	$q = C \frac{\rho_a}{g} (u_* + u_{*th})^2 (u_* - u_{*th})$	1.0	5 – 8
Kawamura (1951)		2.78	14 – 22
Lettau and Lettau (1978)	$q = C \frac{\rho_a}{g} \sqrt{\frac{d_n}{D_n}} (u_* - u_{*th}) u_*^2$	6.7	46 – 75

* Other values are the shear velocity $u_* = \alpha \cdot u_z$ m/s, the shear velocity threshold $u_{*th} = \alpha \cdot 3.87$ m/s, the conversion factor from free-flow wind velocity to shear velocity $\alpha = 0.058$, the air density $\rho_a = 1.25$ kg/m³, the particle density $\rho_p = 2650.0$ kg/m³, the gravitational constant $g = 9.81$ m/s², the nominal grain size $d_n = 335$ μ m, a reference grain size $D_n = 250$ μ m and the height above the bed of the wind measurement $z = 10$ m.

283 to transport both fine sediment and large elements that are considered non-
284 erodible. Moreover, the formulation of Bagnold (1937) overestimates the
285 measured aeolian sediment transport rates in the Sand Motor domain less
286 compared to alternative formulations (Table 1, rightmost column).

287 Water levels and wave heights are initially uniformly imposed to the
288 model. Consequently, the tidal range, mean water level and wave heights
289 that are present at the Sand Motor periphery are also present in the dune
290 lake and lagoon. In reality, the tidal range and wave heights in the dune
291 lake and lagoon are much lower, while the mean water level in the dune lake
292 and lagoon is elevated compared to mean sea level (de Vries et al., 2015). To
293 account for these spatial differences in hydrodynamics a hydrodynamic mask
294 is applied (Figure 4, middle and lower panel).

295 Subtidal changes in topography are not simulated by the model. The sub-
296 tidal changes can be important to aeolian sediment transport as the location
297 and size of aeolian sediment erosion and deposition areas might change. To
298 account for these changes, measured topographies are imposed to the model
299 through a Basic Model Interface (BMI, Peckham et al., 2013).

300 All measured topographies in the period between September 1, 2011 and
301 September 1, 2015 are linearly interpolated in time as to obtain daily up-
302 dates of the Sand Motor’s topography. The hydrodynamic mask is updated
303 along with the topography. The presented aeolian sediment transport rates
304 are based on the time-integrated entrainment and deposition rates that are

305 computed by the model rather than differences in topography.

306 4.3. Calibration

307 The model is calibrated on the shape of roughness elements that emerge
308 from the bed and shelter the sand surface from wind erosion, the drying
309 rate of the soil and the time needed for the sediment transport to adapt to
310 changing wind conditions. These processes are represented in the model by
311 parameters for which data or literature can only provide approximate values:

- 312 1. σ , as used in the formulation of Raupach et al. (1993, Equation 4), is
313 the ratio between the basal and frontal area of the roughness elements
314 that constitute the beach armor layer.
- 315 2. T_{dry} is the time scale at which the beach dries out after flooding (Equa-
316 tion 3). It represents the time in which the soil moisture content halves
317 in case the beach is not inundated and no evaporation occurs.
- 318 3. T is the adaptation time scale in the right-hand side of the advec-
319 tion equation (Equation 2). It represents the time scale to which the
320 sediment transport adapts to variations in the wind conditions and
321 sediment availability.

322 The implementation of roughness elements is characterized by three cal-
323 ibration parameters: m , β and σ (Equation 4). m is a factor to account for
324 the difference between the mean and maximum shear stress and is usually
325 chosen as 0.5 for field applications (Raupach et al., 1993; McKenna Neuman
326 et al., 2012). Numerically it is irrelevant if β or σ is calibrated as they only
327 appear as a ratio $\frac{\beta}{\sigma}$ in the model implementation. As β is the ratio between
328 the drag coefficient of the roughness elements alone and the drag coefficient
329 of the unarmored sandy bed, the value can be assumed to be reasonably
330 generic. In contrast, σ depends on the shape and protrusion of the rough-
331 ness elements and therefore depends on the field site and varies in time.
332 For example, a spherical object placed on top of the bed would be repre-
333 sented by $\sigma = 1$, while a spherical object protruding halfway through the
334 bed (hemisphere) would be represented by $\sigma = 2$. Consequently, calibration
335 of σ seems to be preferable as it is less certain. Wind tunnel experiments
336 presented by McKenna Neuman et al. (2012) investigated the influence of
337 lag deposits, consisting of shells and shell fragments, on aeolian sediment
338 transport. Values for the calibration coefficients m and β were found to be
339 0.5 and 130 respectively and are adopted for the Sand Motor hindcast. An

340 optimal average value for σ is obtained by systematic variation between 2
341 and 20.

342 The drying rate of the beach (T_{dry}) depends on many factors, like grain
343 size, soil moisture content, groundwater level, wind speed and solar radia-
344 tion. The use of a single time scale as aggregate for these processes is an
345 oversimplification of reality. Therefore a wide range of parameter values is
346 covered in the calibration. T_{dry} is varied between 0.1 and 10 hours where the
347 former results in virtually instant drying and the latter results in an inter-
348 tidal beach that is permanently too moist for aeolian sediment transport to
349 be initiated.

350 The adaptation time scale (T), that represents the swiftness of aeolian
351 sediment transport to adapt to changing wind conditions, is in the order of
352 seconds (Davidson-Arnott et al., 2008; de Vries et al., 2014b). As the model
353 time step is orders of magnitude larger, the model effectively solves steady
354 states and the value for T will not affect temporal variations in sediment
355 transport. However, the adaptation time scale also affects the development
356 of the saltation cascade in space. Sediment transport increases in downwind
357 direction from a zero-flux boundary, like the water line in case of onshore
358 wind, with a rate that is governed by the value of T . Consequently, T influ-
359 ences the width of the source area in case of abundant sediment availability.
360 T is varied between 1 and 10 seconds.

361 The calibration is performed based on the bi-monthly erosion and de-
362 position volumes as measured in the Sand Motor domain (Hoonhout and
363 de Vries, 2017). The erosion and deposition volumes are determined within
364 seven predefined zones (Figure 5) that aim to separate areas with marine
365 influences from areas without marine influences, and separate areas with net
366 aeolian erosion from areas with net aeolian deposition. The zonation is based
367 on the 0, 3 and 5 m+MSL contour lines that roughly correspond with the
368 mean water level, maximum runup level or berm edge and the dune foot
369 respectively. The average R^2 value of the time series for erosion and deposi-
370 tion is used as benchmark. The R^2 value represents the fraction of explained
371 variance and is defined as:

$$R^2 = 1 - \frac{\sum_n [V_{\text{measured}}^n - V_{\text{model}}^n]^2}{\sum_n [V_{\text{measured}}^n - \overline{V_{\text{measured}}^n}]^2} \quad (8)$$

372 where V^n is the measured or modeled sediment volume in time period n .
373 The overbar denotes time-averaging. In addition the root-mean-square error

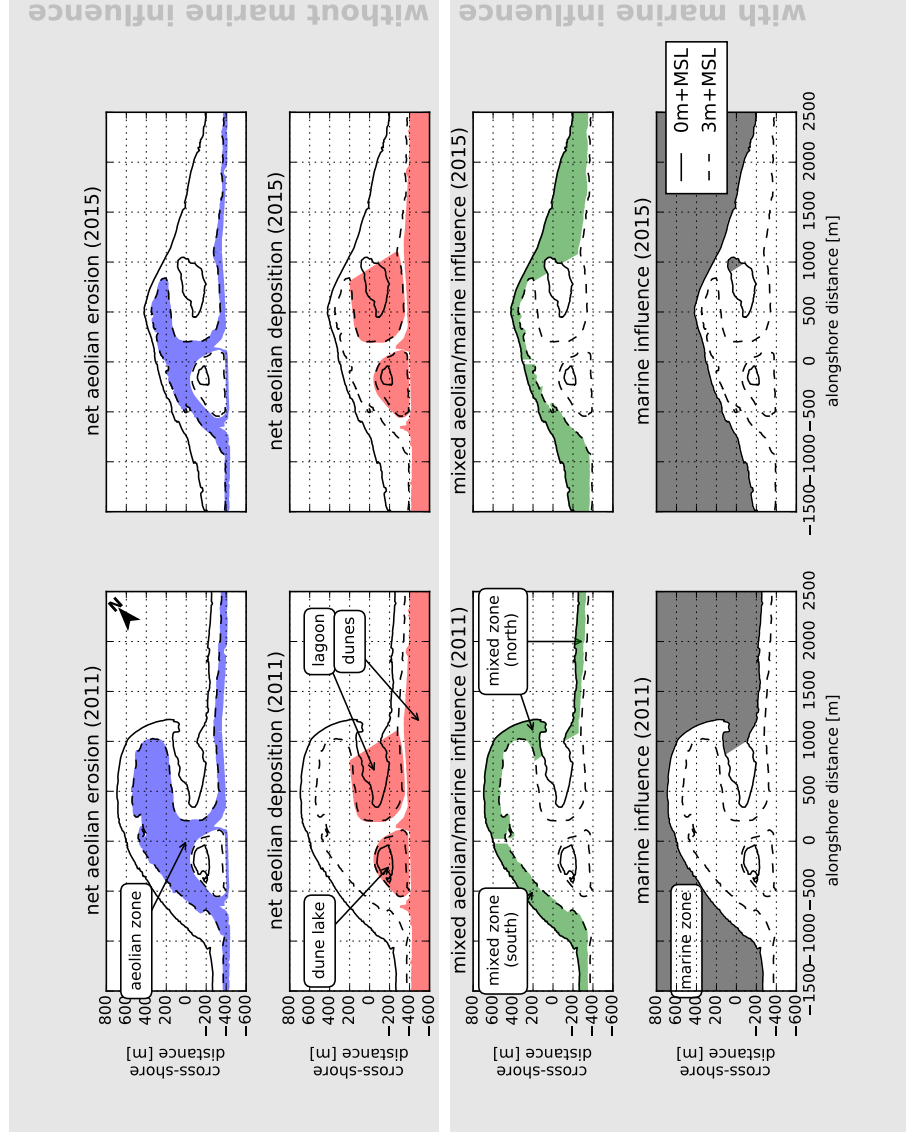


Figure 5: Zonation of the Sand Motor domain into zones with net aeolian erosion and no marine influence, net aeolian deposition and no marine influence, mixed aeolian/marine influence and marine influence. Zonation is based on the 0, 3 and 5 m+MSL contour lines that roughly correspond with the mean water level, maximum runup level or berm edge and the dune foot respectively. Left panels: 2011. Right panels: 2015. Source: Hoonhout and de Vries (2017).

(RMSE) is presented as absolute measure for the model accuracy, which is defined as:

$$RMSE = \sqrt{\sum_n [V_{\text{measured}}^n - V_{\text{model}}^n]^2} \quad (9)$$

The calibration itself is performed in three steps:

1. A coarse calibration on σ and T_{dry} .
2. A calibration on T using the provisional optimal settings for σ and T_{dry} .
3. A fine calibration on σ and T_{dry} using the optimal setting for T .

5. Results

The optimal model settings were chosen from 150 realizations (Figure 6). The optimal realization has an R^2 value of 0.93 and a RMSE of $3 \cdot 10^4 \text{ m}^3$. The corresponding optimal parameter settings are found to be $\sigma = 9.2$, $T_{\text{dry}} = 2 \text{ h}$ and $T = 1 \text{ s}$. These settings were ultimately selected from a cluster of realizations with comparable R^2 values based on the relative sediment supply from the mixed zones (Figure 5, third row) at the end of the simulation. An overview of all model settings for the calibrated model is given in Appendix A.

Figure 7 shows that erosion from the aeolian zone (Figure 5, first row) is most pronounced in the first year and least in the second year in both the measurements and the model results. Also the deposition of aeolian sediment in the dune lake and lagoon (Figure 5, second row) is observed in both the measurements and model results, although the model underestimates these deposited volumes. The deposition in the dune lake and lagoon is also more localized in the measurements than in the model results. The spatial variability in the erosion of the aeolian zone is larger in the measurements than in the model results. The large variability measured in the mixed zone is not present in the model results as hydrodynamic sediment transport is not simulated.

The development of the total erosion and deposition volumes in the Sand Motor domain in the four year period is represented well by the model (Figure 8). The dune accumulation volume is overestimated at the expense of the sediment volumes deposited in the dune lake and lagoon (Figure 9). As the dune area is not included in the model domain, the sediment flux over the onshore boundary is assumed to settle in the dunes entirely. The total

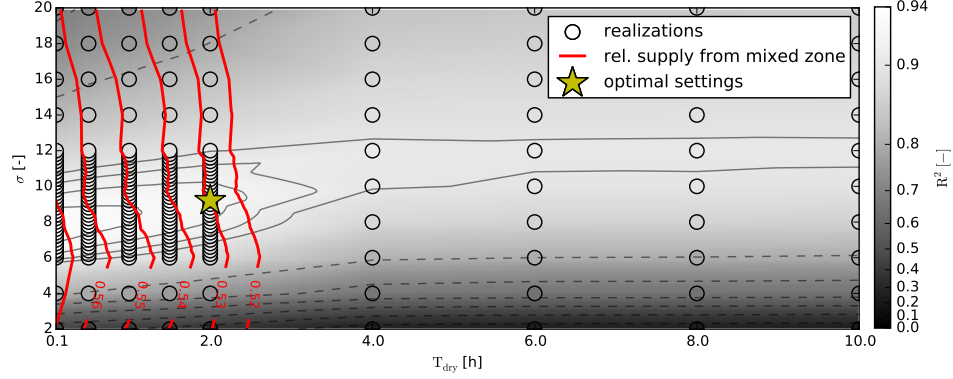


Figure 6: Systematic variation of calibration parameters σ and T_{dry} with $T = 1$ s. The circles indicate the realizations made. The colored background depicts a linear interpolation of the R^2 values with respect to the measurement data presented in Hoonhout and de Vries (2017) and Figure 8. The solid isolines depict R^2 values from 0.90 to 0.93, while the dashed isolines depict R^2 values from 0.0 to 0.9. The red lines depict the relative supply from the mixed zones ranging from 52% to 57%. The yellow star indicates the optimal value model settings.

406 sediment accumulation at the end of the simulation is underestimated by 12%
 407 as the offshore sediment deposits are not included in the large scale sediment
 408 budget analysis that are used for comparison. The underestimation is unique
 409 for the last nine months of the simulation as the model overestimates the
 410 total sediment accumulation with 5% on average (Figure 8). The relative
 411 importance of the mixed zone as supplier of aeolian sediment is well captured.

412 The change in beach height within the most recent 3 m+MSL contour,
 413 that marks the aeolian zone, is represented by the model as the R^2 value is
 414 0.71 and the RMSE is about 4 cm or 12% of the average bed level change
 415 (Figure 10). As the change in beach height is computed within the most
 416 recent 3 m+MSL contour, the discrepancy is illustrative for the differences
 417 in spatial variability in erosion between measurements and model results.
 418 The lowering of the beach in the aeolian zone in the first half year of the
 419 simulation is particularly underestimated, while the accelerated erosion in
 420 this period is well captured in the total sediment transport. This indicates
 421 that sediment is eroded from outside the most recent 3 m+MSL contour.

422 The coverage of non-erodible elements $\lambda\sigma$ [-] (Equation 4) in the aeolian
 423 zone varies between 60% and 80% at the end of the simulation. The coverage
 424 is high compared to the 10% – 20% shell coverage estimated to be present

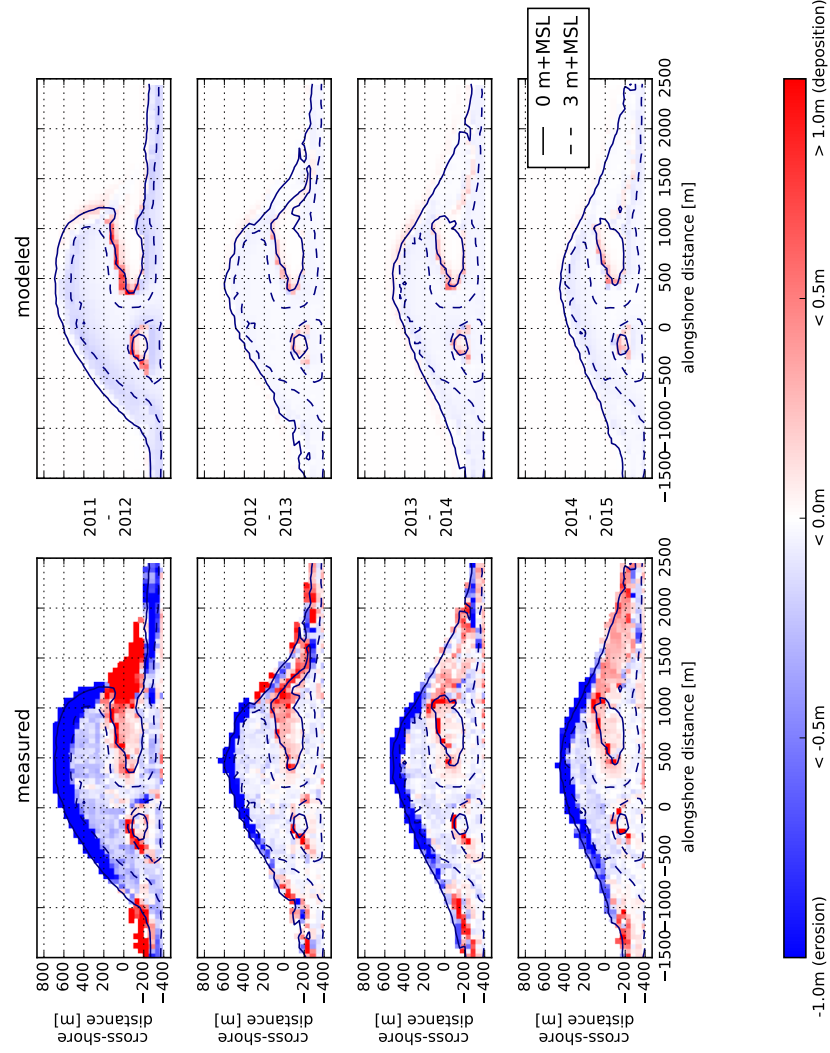


Figure 7: Simulated and measured yearly sedimentation and erosion above 0 m+MSL. Model results only include aeolian sediment transport as hydrodynamic sediment transport is not computed. Comparisons are made between the September surveys of each year.

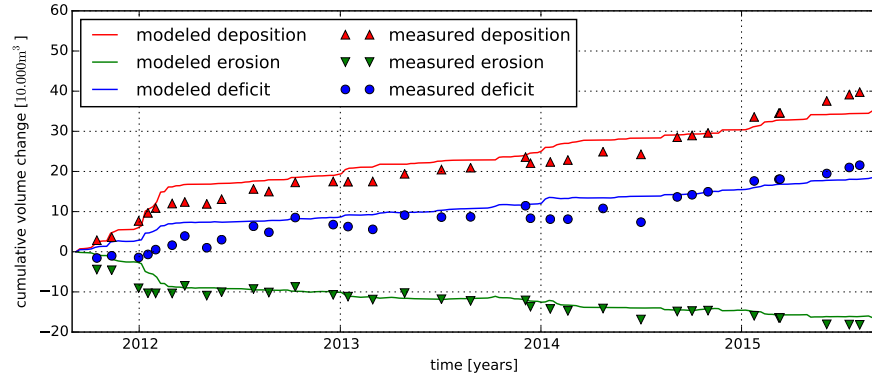


Figure 8: Simulated net volume change of erosion and deposition volumes compared to measured net volume change as presented in Hoonhout and de Vries (2017).

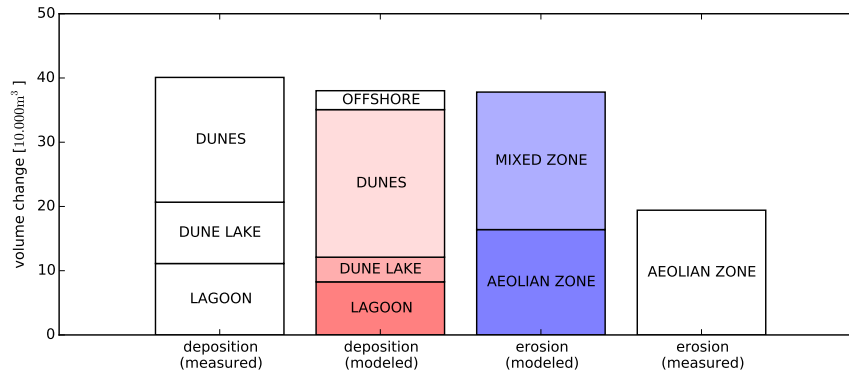


Figure 9: Total erosion and deposition volumes at the end of the simulation and measured total erosion and deposition volumes as presented in Hoonhout and de Vries (2017).

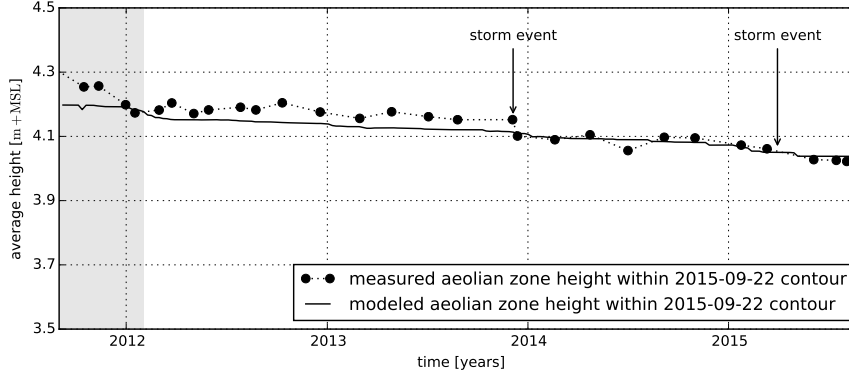


Figure 10: Simulated average beach height in the aeolian zone compared to measured average beach height as presented in Hoonhout and de Vries (2017).

at the Sand Motor above 3 m+MSL based on gridded photographs.

Both the spatial and temporal variations in aeolian sediment availability are crucial for an accurate description of total sedimentation and erosion volumes as well as an accurate prediction of the aeolian sediment source and deposition areas. Figure 11 compares the total sedimentation volume according to measurements, the calibrated model and additional simulations, that are variations of the calibrated model in which spatial and/or temporal variations in the shear velocity threshold are averaged out. During these additional simulations the shear velocity threshold is not computed by the model, but space- and/or time-averaged thresholds based on the model results of the calibrated model are imposed. Negligence of the spatial variations results in a 79% underestimation of the total sedimentation volume and a relative contribution of 8% of the mixed zones. The negligence of the temporal variations results in a 46% overestimation of the total sedimentation volume and a relative contribution of 86% of the mixed zones. In addition, a simulation without limitations in sediment availability overestimates the measured total sedimentation volumes with 400%, which is comparable to the wind transport capacity following Bagnold (1937, Figure 3).

6. Discussion

The model results show that multi-annual aeolian sediment erosion and deposition volumes, and the relative importance of the mixed zones as source

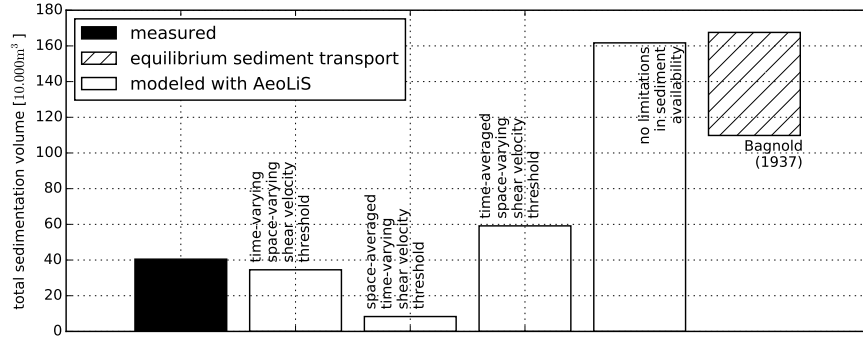


Figure 11: The influence of time-varying and space-varying shear velocity thresholds on the total sedimentation volume. The two leftmost bars depict the measured and modeled sedimentation volume as obtained from the calibrated model (Figure 9). The middle two bars depict results from two separate model simulations in which a space-averaged threshold time series or a time-averaged threshold field is imposed respectively. The threshold averages are based on the result from the calibrated model. The two rightmost columns depict a result from a separate model simulation with a constant uniform threshold based on only a constant uniform median grain size and the estimated equilibrium sediment transport following Bagnold (1937) respectively (Table 1).

446 of aeolian sediment are reproduced with reasonable accuracy. This suggests
447 that indeed significant limitations in sediment availability, due to soil mois-
448 ture content and beach armoring, govern aeolian sediment transport in the
449 Sand Motor domain. A comparison with a simulation without limitation in
450 sediment availability suggests that aeolian sediment availability in the Sand
451 Motor domain is limited to about 25% – 35% of the wind transport capacity.

452 The negligence of spatial variations causes the model to underestimate
453 the measured total sedimentation volume. The sediment supply from the rel-
454 atively small mixed zone is marginalized as the imposed space-averaged shear
455 velocity threshold is relatively high. In contrast, the negligence of temporal
456 variations causes the model to overestimate the measured total sedimenta-
457 tion volume. The sediment supply from the mixed zones is increased as the
458 effect of its periodic flooding is averaged out. At the same time, the sed-
459 iment supply from the aeolian zone is decreased as the influence of beach
460 armoring affects sediment availability from the start of the simulation rather
461 than after the development of the beach armor layer. Therefore, the total
462 sedimentation volume is not only overestimated, but also the importance of
463 the mixed zones as supplier of aeolian sediment.

464 *6.1. Seasonal and local variations in sedimentation and erosion*

465 The model can reproduce multi-annual trends in sedimentation volume,
466 which is the aim of the hindcast, but seasonal and local variations are some-
467 times not represented by the model. An analysis of these variations is inter-
468 esting as they influence the accuracy of specific model results.

469 Average wind speeds tend to be elevated in December and January (Fig-
470 ure 2), which leads to short periods of accelerated sediment accumulation in
471 the beginning of 2012, 2013 and 2015 that are captured well by the model.
472 Early 2014 no accelerated sediment accumulation is measured, while the
473 model simulation shows an increase in sediment accumulation originating
474 from the mixed zones similar to other years.

475 The discrepancy early 2014 might be explained by topographic changes
476 induced by hydrodynamic forces. On December 5th, 2013 an exceptional
477 storm hit the Dutch coast. During this storm a significant decrease in aeolian
478 deposits in the lagoon was observed, while deposits in the dunes and dune lake
479 increased only marginally. The assumption that the closed end of the lagoon
480 is mainly governed by aeolian sediment transport might be violated in these
481 exceptional conditions. At the same time, the erosion of the aeolian zone that
482 day equaled the total erosion of the aeolian zone that year. Consequently, the

total subaerial sediment volume decreased that day with about $1 \cdot 10^4 \text{ m}^3$, possibly caused by hydrodynamic forces. This suggests that the simplified hydrodynamics, despite the use of a hydrodynamic mask, are a limiting factor in describing the Sand Motor’s subaerial morphodynamics during extreme storms.

In the first months of the simulation, the total sediment accumulation is well represented, but erosion of the aeolian zone is underestimated. As beach armoring is the most important availability limitation in the aeolian zone, this suggests that the armoring rate is overestimated by the model. The armoring rate is mainly influenced by initial shell fraction of 5%, which might be overestimated. Alternatively, the initially uniform distribution of shells in the bed is not an accurate representation of reality.

Measured erosion and deposition rates exceed modeled erosion and deposition rates in the final nine months of the simulation. In this period dune growth seems to accelerate, while neither the deposition in the dune lake and lagoon did accelerate nor did the wind speed increase. The apparent acceleration is therefore solely found in the half yearly lidar measurements of the dune area (Hoonhout and de Vries, 2017) and is consequently based on a single data point. Despite the uncertainty involved in the measured acceleration, also precipitation rates, that were up to 70% lower in this period compared to the same period in other years, might explain the discrepancy at the end of the simulation (Jackson and Nordstrom, 1998). For the hindcast no precipitation time series are imposed as the effect on the aeolian sediment transport rate is not properly understood yet. Consequently, the calibration of the model might have resulted in an overestimated importance of beach armoring to compensate for the negligence of precipitation.

The distribution of the aeolian sediment deposits over the dune lake, lagoon and dunes is not represented well as deposits in the dune lake and lagoon are underestimated. Additional hydrodynamic and hydrologic processes, like wind setup and groundwater seepage, might cause the entrapment area in reality to be larger than modeled. But more importantly, the dune lake and lagoon are positioned in the lee of the Sand Motor crest with respect to the predominant southwesterly wind direction. The height difference between the Sand Motor crest and the water level in the lagoon and dune lake is several meters, which is likely to influence the local wind field significantly. The probable decrease in wind shear in the lee of the Sand Motor crest promotes deposition of aeolian sediment and likely hampers supply to the dunes. These local variations in wind shear are not included in the simulations.

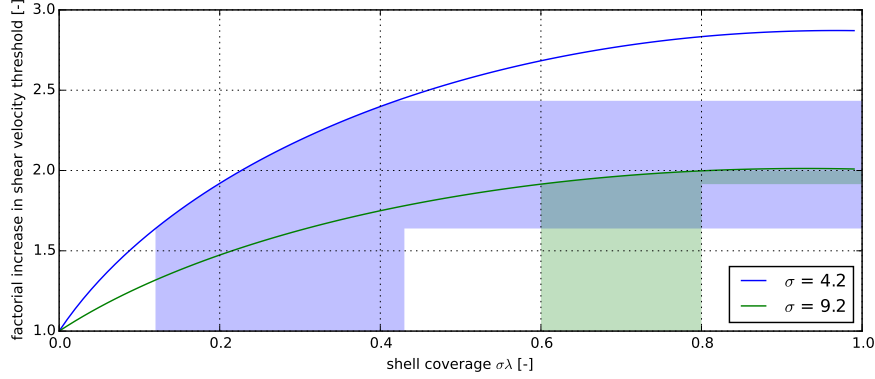


Figure 12: Relation between shear velocity threshold, shell coverage and σ according to Raupach et al. (1993, Equation 4). The shaded areas indicate the relevant parameter ranges from McKenna Neuman et al. (2012) (blue) and the model results (green).

521 6.2. Beach armoring, sediment availability and the shear velocity threshold

522 The influence of beach armoring is reflected in the model by both σ and
523 the roughness density λ (Equation 4). The optimal value for σ was found to
524 be 9.2, which is high compared to the value of 4.2 found by McKenna Neuman
525 et al. (2012). The difference suggests that the roughness elements at the Sand
526 Motor protrude less from the bed compared to what was found in the wind
527 tunnel experiments. Consequently, the importance of beach armoring would
528 be relatively low at the Sand Motor. However, the low σ value is largely
529 compensated by the roughness density λ reflected in a shell coverage $\sigma\lambda$
530 that is high compared to what was found in the wind tunnel experiments
531 (12% – 43% on average) and what is found at the Sand Motor field site
532 (10% – 20%). Figure 12 shows that the combination of high shell coverage
533 and σ value results in a very similar increase of the shear velocity threshold
534 compared to the wind tunnel experiments presented by McKenna Neuman
535 et al. (2012).

536 The reason that the model calibration resulted in this particular value
537 for σ is that the model does not differentiate between the fluid and impact
538 velocity threshold. Therefore, the roughness elements in the model affect
539 the initiation of sediment transport equal to the continuation of sediment
540 transport. The potential reduction in sediment availability increases with a
541 decreasing value for σ (if $m = 0.5$, Figure 12) and is implemented through an
542 increase in shear velocity threshold. The shear velocity threshold also affects

aeolian sediment already in transport and originating from upwind, unarmored beach areas, like the mixed zones. Sediments from upwind areas are therefore partially deposited in the aeolian zone as soon a beach armor layer develops. For low values for σ the local deposition of sediment from upwind areas is already significant with low shell coverage. Low σ values therefore reduce the total sediment accumulation in the dunes quickly. In order for the model to provide reasonable total sediment transport rates, a higher value for σ was found in the calibration that ultimately induces a higher shell coverage. The value for σ therefore does not only represent a spatiotemporal averaged emergence of roughness elements, but also a compromise between its effect on the fluid and impact velocity threshold.

Note that the model conceptually allows to differentiate between the impact and fluid threshold. The right-hand side of the advection equation (Equation 2) can be modified according to:

$$E_k - D_k = \min \left(\frac{\partial m_{a,k}}{\partial t} \quad ; \quad \frac{\hat{w}_k}{T} \cdot [(1 - S_k) \cdot c_{\text{sat},k}^{\text{fluid}} + S_k \cdot c_{\text{sat},k}^{\text{impact}} - c_k] \right) \quad (10)$$

where $c_{\text{sat},k}^{\text{fluid}}$ [kg/m²] and $c_{\text{sat},k}^{\text{fluid}}$ [kg/m²] are the sediment transport capacity associated with the fluid and impact threshold respectively and S_k [-] is the degree of saturation.

Unfortunately, empirical data to quantify the differentiation is lacking. This potential model improvement is therefore still hypothetical and requires fundamental research on the impact and fluid shear velocity threshold under varying conditions.

7. Conclusions

The Sand Motor hindcast shows that the reduction of aeolian sediment availability due to soil moisture and beach armoring can largely explain the low accumulation volumes in the Sand Motor domain. The AEOLIS model has shown to be quantitatively valuable and practically applicable. The model provides a framework for the description of complex spatiotemporal variations in aeolian sediment availability and its relation to sediment transport that has not yet been exploited in full.

From the hindcast the following conclusions can be drawn:

- 573 • The AEOLiS model is able to reproduce multi-annual aeolian sediment
574 transport rates in the Sand Motor domain in the four years after its
575 construction with a RMSE of $3 \cdot 10^4 \text{ m}^3$ and R^2 of 0.93 when time series
576 of measured and modeled total aeolian sediment transport volumes are
577 compared.
- 578 • The AEOLiS model is able to reproduce large scale spatial patterns in
579 aeolian sediment transport in the Sand Motor domain in the four years
580 after its construction, but underestimates the deposition in the dune
581 lake and lagoon, likely due to wind setup and groundwater seepage that
582 are not included in the model.
- 583 • The AEOLiS model overestimates the total sedimentation volume with
584 5% on average, but underestimates the total sedimentation volume with
585 12% at the end of the simulation. The discrepancy at the end of the
586 simulation might be caused by a particularly dry season as precipitation
587 is not included in the simulations.
- 588 • The AEOLiS model is able to capture the seasonal variations in sed-
589 iment transport in all years, except for early 2014 when significant
590 morphological change is possibly related to hydrodynamic sediment
591 transport that is not included in the simulations.
- 592 • The AEOLiS model overestimates the shell coverage, which compen-
593 sates the high value for σ . The high σ value is a compromise between
594 the fluid and impact threshold that are currently assumed to be equal.
- 595 • The combination of spatial and temporal variations in aeolian sediment
596 availability, due to the combined influence of soil moisture, sediment
597 sorting and beach armoring, and the feedback between aeolian sediment
598 availability and transport is essential for an accurate estimate of the
599 total sedimentation volume and the corresponding aeolian sediment
600 source areas in the Sand Motor domain.

601 Acknowledgements

602 The work discussed in this paper is supported by the ERC-Advanced
603 Grant 291206 – Nearshore Monitoring and Modeling (NEMO) and Deltares.

604 A. Model settings

605 The model schematizations presented in this paper used the settings listed
606 below. Some model settings belong to experimental features of the model and
607 are not discussed. These settings are listed for completeness only and marked
608 with an asterisk (*). The model settings are chosen such that experimental
609 features are disabled.

Parameter	Value			
A	0.085			
CFL	1.0			
Cb	1.5			
T	1.0			
Tdry	5400.0			
Tsalt*	0.0			
accfac	1.0			
bedupdate	False			
beta	130.0			
bi	0.05			
boundary_lateral	circular			
boundary_offshore	noflux			
boundary_onshore	gradient			
callback	None			
cpair	0.0010035			
csalt*	0.035			
dt	3600.0			
eps	0.001			
evaporation	True			
facDOD	0.1			
g	9.81			
gamma	0.5			
grain_dist	0.005709	0.234708	0.608887	0.099666
	0.001029	0.000001	0.010486	0.028503
	0.010486	0.000522	0.000004	
	0.000177	0.000250	0.000354	0.000500
grain_size	0.000707	0.001000	0.002000	0.004000
	0.008000	0.016000	0.032000	
k	0.01			
layer_thickness	0.01			

Parameter	Value	(continued)
m	0.5	
max_error	0.000001	
max_iter	1000	
method_moist	belly_johnson	
method_transport	bagnold	
mixtoplayer	True	
nfractions	11	
nlayers	10	
output_times	604800.0	
porosity	0.4	
restart	None	
rhoa	1.25	
rhop	2650.0	
rhow	1025.0	
runup	False	
scheme	euler_backward	
sigma	11.9	
th_bedslope	False	
th_grainsize	True	
th_humidity*	False	
th_moisture	True	
th_roughness	True	
th_salt*	False	
tstart	0.0	
tstop	126230400.0	
z	10.0	

610 References

- 611 Aagaard, T. (2014). Sediment supply to beaches: Cross-shore sand transport
612 on the lower shoreface. *Journal of Geophysical Research*, 119(4):913–926.
613 doi:10.1002/2013JF003041. 2013JF003041.
- 614 Arens, S. M. (1996). Patterns of sand transport on vegetated foredunes.
615 *Geomorphology*, 17:339–350.
- 616 Baas, A. C. (2002). Chaos, fractals and self-organization in coastal geomor-

- 617 phology: simulating dune landscapes in vegetated environments. *Geomor-*
618 *phology*, 48(1-3):309–328. doi:10.1016/S0169-555X(02)00187-3.
- 619 Bagnold, R. (1937). The transport of sand by wind. *Geographical journal*,
620 pages 409–438.
- 621 Bauer, B. O. and Davidson-Arnott, R. G. D. (2002). A general framework
622 for modeling sediment supply to coastal dunes including wind angle, beach
623 geometry, and fetch effects. *Geomorphology*, 49:89–108. doi:10.1016/S0169-
624 555X(02)00165-4.
- 625 Belly, P. Y. (1964). Sand movement by wind. Technical Report 1, U.S. Army
626 Corps of Engineers CERC, Vicksburg, MS. 38 pp.
- 627 Davidson-Arnott, R. G. D. and Bauer, B. O. (2009). Aeolian sediment trans-
628 port on a beach: Thresholds, intermittency, and high frequency variability.
629 *Geomorphology*, 105:117–126. doi:10.1016/j.geomorph.2008.02.018.
- 630 Davidson-Arnott, R. G. D., Yang, Y., Ollerhead, J., Hesp, P. A., and Walker,
631 I. J. (2008). The effects of surface moisture on aeolian sediment transport
632 threshold and mass flux on a beach. *Earth Surface Processes and Land-*
633 *forms*, 33(1):55–74. doi:10.1002/esp.1527.
- 634 de Schipper, M. A., de Vries, S., Ruessink, G., de Zeeuw, R. C., Rutten, J.,
635 van Gelder-Maas, C., and Stive, M. J. (2016). Initial spreading of a mega
636 feeder nourishment: Observations of the sand engine pilot project. *Coastal*
637 *Engineering*, 111:23–38. doi:10.1016/j.coastaleng.2015.10.011.
- 638 de Vries, S., Arens, S. M., de Schipper, M. A., and Ranasinghe, R. (2014a).
639 Aeolian sediment transport on a beach with a varying sediment supply.
640 *Aeolian Research*, 15:235–244. doi:10.1016/j.aeolia.2014.08.001.
- 641 de Vries, S., Radermacher, M., de Schipper, M., and Stive, M. (2015). Tidal
642 dynamics in the Sand Motor lagoon. In *E-proceedings of the 36th IAHR*
643 *World Congress*.
- 644 de Vries, S., van Thiel de Vries, J. S. M., van Rijn, L. C., Arens, S. M.,
645 and Ranasinghe, R. (2014b). Aeolian sediment transport in supply limited
646 situations. *Aeolian Research*, 12:75–85. doi:10.1016/j.aeolia.2013.11.005.

- 647 Durán, O. and Moore, L. J. (2013). Vegetation controls on the maximum size
648 of coastal dunes. *Proceedings of the National Academy of Sciences of the*
649 *United States of America*, 110:17217–17222. doi:10.1073/pnas.1307580110.
- 650 Dyer, K. R. (1986). *Coastal and estuarine sediment dynamics*. Wiley, Chich-
651 ester.
- 652 Hoonhout, B. M. and de Vries, S. (2016). A process-based model for aeolian
653 sediment transport and spatiotemporal varying sediment availability. *Jour-*
654 *nal of Geophysical Research: Earth Surface*. doi:10.1002/2015JF003692.
655 2015JF003692.
- 656 Hoonhout, B. M. and de Vries, S. (2017). Aeolian sediment supply at a mega
657 nourishment. *Coastal Engineering*. doi:10.1016/j.coastaleng.2017.03.001.
658 Submitted.
- 659 Horikawa, K., Hotta, S., Kubota, S., and Katori, S. (1983). On the sand
660 transport rate by wind on a beach. *Coastal Engineering in Japan*, 26:101–
661 120.
- 662 Hotta, S., Kubota, S., Katori, S., and Horikawa, K. (1984). Sand transport
663 by wind on a wet sand beach. In *Proceedings of the 19th Conference on*
664 *Coastal Engineering*, pages 1264–1281, Houston, TX. ASCE.
- 665 Howard, A. D. (1977). Effect of slope on the threshold of mo-
666 tion and its application to orientation of wind ripples. *Geolog-*
667 *ical Society of America Bulletin*, 88(6):853–856. doi:10.1130/0016-
668 7606(1977)88;853:EOSOTT;2.0.CO;2.
- 669 Huisman, B., De Schipper, M., and Ruessink, B. (2016). Sediment sorting at
670 the sand motor at storm and annual time scales. *Marine Geology*, 381:209–
671 226. doi:10.1016/j.margeo.2016.09.005.
- 672 Jackson, D. W. T. and Cooper, J. A. G. (1999). Beach fetch distance and ae-
673olian sediment transport. *Sedimentology*, 46:517–522. doi:10.1046/j.1365-
674 3091.1999.00228.x.
- 675 Jackson, N. L. and Nordstrom, K. F. (1998). Aeolian transport of sediment
676 on a beach during and after rainfall, wildwood, nj, usa. *Geomorphology*,
677 22(2):151–157. doi:10.1016/S0169-555X(97)00065-2.

- 678 Johnson, J. W. (1965). Sand movement on coastal dunes. Technical Report
679 570, Symp. 3, Paper no. 75, U.S. Department of Agriculture, Washington.
680 pp 747-755.
- 681 Kawamura, R. (1951). Study of sand movement by wind. Technical Re-
682 port HEL-2-8, Hydraulics Engineering Laboratory, Univeristy of Califor-
683 nia, Berkeley.
- 684 Keijsers, J., De Groot, A., and Riksen, M. (2016). Modeling the bio-
685 geomorphic evolution of coastal dunes in response to climate change.
686 *Journal of Geophysical Research: Earth Surface*, 121(6):1161–1181.
687 doi:10.1002/2015JF003815.
- 688 King, J., Nickling, W. G., and Gillies, J. A. (2005). Representation of vege-
689 tation and other nonerodible elements in aeolian shear stress partitioning
690 models for predicting transport threshold. *Journal of Geophysical Re-*
691 *search*, 110(F4). doi:10.1029/2004JF000281. F04015.
- 692 Kroy, K., Sauermann, G., and Herrmann, H. J. (2002). Mini-
693 mal model for sand dunes. *Physical Review Letters*, 88(5):054301.
694 doi:10.1103/PhysRevLett.88.054301.
- 695 Lettau, K. and Lettau, H. (1978). *Exploring the World's Driest Climate.*,
696 chapter Experimental and micrometeorological field studies of dune mi-
697 gration., pages 110–147. University of Wisconsin - Madison. IES Report
698 101,.
- 699 Lynch, K., Jackson, D. W. T., and Cooper, J. A. G. (2008). Aeolian fetch
700 distance and secondary airflow effects: the influence of micro-scale vari-
701 ables on meso-scale foredune development. *Earth Surface Processes and*
702 *Landforms*, 33(7):991–1005. doi:10.1002/esp.1582.
- 703 McKenna Neuman, C., Li, B., and Nash, D. (2012). Micro-
704 topographic analysis of shell pavements formed by aeolian transport in
705 a wind tunnel simulation. *Journal of Geophysical Research*, 117(F4).
706 doi:10.1029/2012JF002381. F04003.
- 707 Nickling, W. G. and Ecclestone, M. (1981). The effects of soluble salts on
708 the threshold shear velocity of fine sand. *Sedimentology*, 28:505–510.

- 709 Peckham, S. D., Hutton, E. W. H., and Norris, B. (2013). A component-based
710 approach to integrated modeling in the geosciences: The design of CSDMS.
711 *Computers and Geosciences*, 53:3–12. doi:10.1016/j.cageo.2012.04.002.
- 712 Radermacher, M., de Schipper, M. A., Swinkels, C., MacMahan, J. H.,
713 and Reniers, A. J. (2017). Tidal flow separation at protruding beach
714 nourishments. *Journal of Geophysical Research: Oceans*, 122(1):63–79.
715 doi:10.1002/2016JC011942.
- 716 Raupach, M., Gillette, D., and Leys, J. (1993). The effect of roughness
717 elements on wind erosion threshold. *Journal of Geophysical Research: At-*
718 *mospheres*, 98(D2):3023–3029. doi:10.1029/92JD01922.
- 719 Sherman, D. J., Jackson, D. W., Namikas, S. L., and Wang, J. (1998).
720 Wind-blown sand on beaches: an evaluation of models. *Geomorphology*,
721 22(2):113–133. doi:10.1016/S0169-555X(97)00062-7.
- 722 Sherman, D. J. and Li, B. (2012). Predicting aeolian sand trans-
723 port rates: a reevaluation of models. *Aeolian Research*, 3(4):371–378.
724 doi:10.1016/j.aeolia.2011.06.002.
- 725 Stive, M. J. F., de Schipper, M. A., Luijendijk, A. P., Aarninkhof, S. G. J.,
726 van Gelder-Maas, C., van Thiel de Vries, J. S. M., de Vries, S., Henriquez,
727 M., Marx, S., and Ranasinghe, R. (2013). A new alternative to saving our
728 beaches from sea-level rise: the Sand Engine. *Journal of Coastal Research*,
729 29(5):1001–1008. doi:10.2112/JCOASTRES-D-13-00070.1.
- 730 Stockdon, H. F., Holman, R. A., Howd, P. A., and Sallenger, A. H. (2006).
731 Empirical parameterization of setup, swash, and runup. *Coastal engineer-*
732 *ing*, 53(7):573–588. doi:10.1016/j.coastaleng.2005.12.005.
- 733 Van Boxel, J., Arens, S., Van Dijk, P., et al. (1999). Aeolian pro-
734 cesses across transverse dunes. i: Modelling the air flow. *Earth Sur-*
735 *face Processes and Landforms*, 24(3):255–270. doi:10.1002/(SICI)1096-
736 9837(199903)24:3<255::AID-ESP962>3.0.CO;2-3.
- 737 Van Dijk, P., Arens, S., Van Boxel, J., et al. (1999). Aeolian processes
738 across transverse dunes. ii: Modelling the sediment transport and pro-
739 file development. *Earth surface processes and landforms*, 24(4):319–333.
740 doi:10.1002/(SICI)1096-9837(199904)24:4<319::AID-ESP963>3.3.CO;2-D.

⁷⁴¹ Weng, W. S., Hunt, J. C. R., Carruthers, D. J., Warren, A., and Wiggs, G.
⁷⁴² F. S. (1991). Air flow and sand transport over sand-dunes. *Acta Mechanica*,
⁷⁴³ 2:1–22.